Nanoscale

Accepted Manuscript

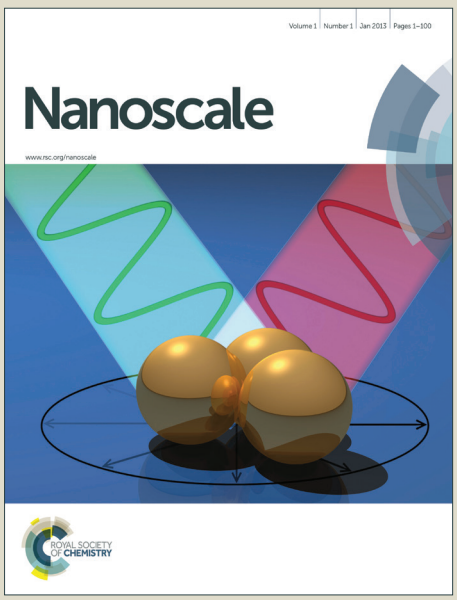

ROYAL SOCIETY OF CHEMISTRY

www.rsc.org/nanoscale

Journal Name

RSCPublishing

ARTICLE

Ethylenediamine-mediated synthesis of Mn_3O_4 nano-octahedrons and their performance as electrocatalysts for oxygen evolution reaction

Cite this: DOI: 10.1039/xoxxoooooox

Received ooth January 2012,
Accepted ooth January 2012

DOI: 10.1039/xoxxoooooox

www.rsc.org/

Chun Xian Guo, Shucheng Chen and Xianmao Lu*

Mn_3O_4 octahedrons with well-defined facets exhibit enhanced catalytic activity and sensing characteristics and have attracted much attention in recent years. However, current fabrication methods for Mn_3O_4 octahedrons generally produce particles with sizes in the micron and sub-micron scales; and impurities such as MnO_2 and Mn_2O_3 are often found. We present the synthesis of Mn_3O_4 nano-octahedrons with pure Mn_3O_4 phase and size down to 50 nm based on a hydrothermal method using $Mn(NO_3)_2$ as the manganese source and ethylenediamine (EDA) as the structure-mediating agent. It is found that EDA plays a critical role in the formation of Mn_3O_4 nano-octahedrons in dictating both the morphology and the crystal structure of the products. The growth process is proposed to follow a "dissolution-recrystallization" and "capping-molecule assisted growth" mechanism. As electrocatalysts towards oxygen evolution reaction, the 50-nm Mn_3O_4 nano-octahedrons demonstrate a considerably enhanced activity compared to 160-nm Mn_3O_4 octahedrons.

1. Introduction

Controlling the size and shape of nanomaterials to achieve desired properties is an important scientific goal which could impact both fundamental understanding of their growth mechanisms and a wide range of technological applications.[1-7] For catalytic reactions, in particular, nanomaterials with small sizes and favourable shapes could provide high specific surface areas and desired exposed facets that allow much enhanced activity.[8-15] One example of such materials is Mn_3O_4. As the most stable form of manganese oxides at high temperature, Mn_3O_4 has a low resistivity, which is an essential characteristic for electrode materials in catalytic reactions.[16-28] Therefore, Mn_3O_4 has been widely used as electrocatalysts for a number of reactions including photochemical water oxidation, oxygen reduction reaction, and carbon monoxide oxidation.[19-21] For these and many other catalytic reactions, the size and shape of Mn_3O_4 nanocatalysts are critical factors that considerably affect the performance. For example, 7.9-nm Mn_3O_4 nanocrystals show much higher catalytic activity towards the decomposition of hydrogen peroxide than 12.6-nm ones (more than 50% increase of rate constant).[22] In addition, among Mn_3O_4 nanocrystals with different shapes, Mn_3O_4 octahedrons with high-index facets exhibit high photodecomposition activity, enhanced sensing characteristics, and improved electrochemical energy storage.[11,26,29-32] Therefore, the synthesis of Mn_3O_4 octahedrons has attached much attention. Very recently, using $KMnO_4$ as the manganese source and polyethylene glycol as the reducing agent, Mn_3O_4 octahedrons with size of around 150 nm have been synthesized by Li and coworkers with a hydrothermal method.[11] The 150-nm Mn_3O_4 octahedrons exhibit enhanced catalytic activity than commercial Mn_3O_4 powders towards the photodecomposition of rhodamine B. In addition to catalytic applications, Mn_3O_4 octahedrons have also found applications in sensing and energy storage. For instance, Zhang *et al.* have fabricated Mn_3O_4 octahedrons with sizes in the range of 1-3 μm by reducing $KMnO_4$ in the presence of dodecylamine, Na_2SO_3, and ethanol.[30] The resulting Mn_3O_4 micro-octahedrons exhibit a higher response and better stability towards acetone molecule sensing than Mn_3O_4 hexagonal nanoplates. It is believed that the high Miller indices of the exposed facets of the Mn_3O_4 micro-octahedrons contribute to the improved sensing performance. Mn_3O_4 octahedrons with sizes of around 160 nm have also been prepared recently via the reduction of $KMnO_4$ using ethylenediaminetetraacetic acid disodium salt with the assistance of nitric acid.[26] As a supercapacitor electrode material, the 160-nm Mn_3O_4 octahedrons demonstrated an enhanced specific capacitance compared to the other Mn_3O_4 nanomaterials.

Despite the recent progress in the preparation of Mn_3O_4 octahedrons, the sizes obtained are typically in the micron- and sub-micron scales. Because materials with smaller sizes can provide higher surface/volume ratio and much enhanced chemical reactivity,[25,26] Mn_3O_4 octahedrons at nanoscale are more favorable for various applications. Particularly for catalysis, Mn_3O_4 nano-octahedrons would allow increased number of active sites and thus enhanced interaction with reactive molecules. In this work, we present the synthesis of Mn_3O_4 nano-octahedrons with sizes down to 50 nm based on a hydrothermal method using $Mn(NO_3)_2$ as the manganese source and ethylenediamine (EDA) as the structure-mediating agent. It was found that EDA plays a critical role in dictating both the

morphology and the crystal structure of the products. As a demonstration, the Mn_3O_4 nano-octahedrons were used as an electrocatalyst towards oxygen evolution reaction (OER). An enhanced OER performance was attained for the 50-nm Mn_3O_4 nano-octahedrons compared to that of 160-nm Mn_3O_4 octahedrons. The OER activity of 50-nm Mn_3O_4 nano-octahedrons is also compared with that of some recently reported Ni-, Pt-, Ru- and Ir-based OER catalysts.

2. Experimental section

Materials

All chemicals, including $Mn(NO_3)_2$, ethylenediamine, ethylenediaminetetraacetic acid disodium salt, nitric acid, $KMnO_4$ and Nafion, were purchased from Sigma-Aldrich and used as received.

Synthesis of 50-nm octahedral Mn_3O_4

In a typical synthesis of 50-nm octahedral Mn_3O_4, 20 ml of 10 mM $Mn(NO_3)_2$ solution was first loaded in a 50 mL autoclave and purged with N_2 for 15 min. In the meantime, 20 ml of 10 mM EDA solution was purged with N_2 in a glass baker for 15 min before it was added to the $Mn(NO_3)_2$ solution. The nitrogen purging was kept for another 15 min. The autoclave was then sealed and heated up to 180 °C. The reaction was allowed to proceed at 180 °C for 4 h. After cooling down to room temperature, the material was collected by centrifugation and washed with water for three times. Finally the obtained precipitate was dried in air at 60 °C for 6 h.

Synthesis of 160-nm octahedral Mn_3O_4

Large Mn_3O_4 octahedrons (~160 nm) were synthesized according to a recent work.[26] Briefly, 2 ml of 0.5 M ethylenediaminetetraacetic acid disodium salt and 5 ml of 0.2 M $KMnO_4$ aqueous solution were loaded into a 50-mL autoclave, followed by the addition of 28 mL water. The pH of the solution was then adjusted to 6.0 using 2 M HNO_3 aqueous solution under stirring. The autoclave was sealed and heated at 180 °C for 4 h. Once it was cooled down to room temperature, the product was collected via centrifugation, followed by washing and drying.

Material characterizations

The crystal structure of the composite was characterized with powder X-ray diffraction (XRD, Bruker D8 ADVANCE X-ray diffractometer). Transmission electron microscopy (TEM) images were recorded on a JEM-2100F electron microscope operating at an accelerating voltage of 200 kV. Field-emission scanning electron microscopy (FESEM) images were recorded using a JEOL JSM-6700F scanning electron microscope. X-ray photoelectron spectroscopy (XPS) characterizations were performed on a PHI Quantera x-ray photoelectron spectrometer with a chamber pressure of 5×10^{-9} torr, a spatial resolution of 30 μm and an Al cathode as the X-ray source.

Oxygen evolution reaction tests

Catalyst inks were prepared by mixing oxide samples with carbon black XC72 at a 5:1 mass ratio (oxide/carbon), followed by sonicating in 5 mL tetrahydrofuran solution containing Nafion 117 solution. The concentrations of the components are as follows: 5 mg mL^{-1} for oxide, 1 mg mL^{-1} for carbon black, and 1 mg mL^{-1} for Nafion. Glassy carbon electrodes with an area of 0.196 cm^2 were polished to a mirror finish with 0.3 and 0.05 μm alumina slurries. Then, 10 μL catalyst ink was drop-cast onto a rotating disk electrode before it was allowed to dry overnight in a sealed glass baker saturated with tetrahydrofuran vapor to form a homogeneous thin film catalyst coating. All electrochemical tests were performed with 3-electrode cell configuration using an Autolab PGSTAT128N potentiostat. Saturated calomel electrode (SCE) and Pt foil were used as the reference and counter electrode, respectively. Curves were measured at 1600 rpm with a scan rate of 5 mV s^{-1} in 0.1 M KOH electrolyte.

3. Results and discussion

3.1 Structural characterization

The field-emission scanning electron microscopy (FESEM) image of the Mn_3O_4 nano-octahedrons shows uniform size and high yield (**Figure 1a**). FESEM images at high magnification reveal that the Mn_3O_4 particles have a well-defined octahedral shape (Figure 2b and Figure S1) with a mean edge length of 50 nm. X-ray diffraction (XRD) pattern exhibits strong diffraction peaks, indicating that the prepared product is highly crystalline. All peaks match perfectly with tetragonal Mn_3O_4 (hausmannite), which has a space group of $I4_1/amd$ and lattice parameters of a = b = 5.762 Å and c = 9.461 Å (PDF 01-070-9110). No peaks from other forms of manganese oxides were observed. Based on peak broadening, the particle size was estimated to be 49.5 nm using Scherrer formula,[33] consistent with FESEM observation. To investigate the oxidation states of Mn in the product, X-ray photoelectron spectroscopy (XPS) spectrum was acquired with the Mn 2*p* peak given in Figure 1d. The binding energy of Mn $2p_{3/2}$ is 641.08 eV, and the spin orbit splitting between the Mn $2p_{3/2}$ and Mn $2p_{1/2}$ level is 11.65 eV, both agreeing well with Mn_3O_4.[34] The XRD and XPS results confirm that the product is pure Mn_3O_4.

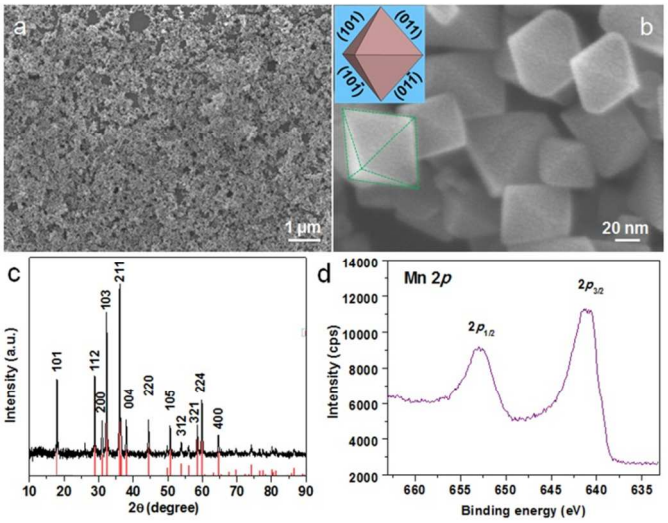

Fig. 1 a and b) FESEM images with different magnifications of the synthesized Mn_3O_4 nano-octahedrons. Inset of b) illustrates the octahedral shape and the exposed facets. c) XRD pattern and d) XPS Mn 2*p* spectrum of the as-synthesized material.

Transmission electron microscopy (TEM) image in **Figure 2a** further confirms the octahedral shape of the as-prepared Mn_3O_4 nanocrystals and also their nanoscale size. TEM images with high magnification in Figure 2b and 2c indicate high crystallinity of the Mn_3O_4 nano-octahedrons. The lattice fringes

of the Mn_3O_4 nano-octahedrons were well-resolved. The measured *d*-spacing of 0.49 nm matches well with that of (011) planes of tetragonal Mn_3O_4.[35] This is further confirmed from the corresponding Fast Fourier Transform (FFT) pattern in Figure 2d. To better understand the structure, the spinel crystal structure of Mn_3O_4 with a space group of $I4_1/amd$ is illustrated in Figure 3f, in which Mn^{2+} ions are located at the tetrahedral site and Mn^{3+} ions at the octahedral site.

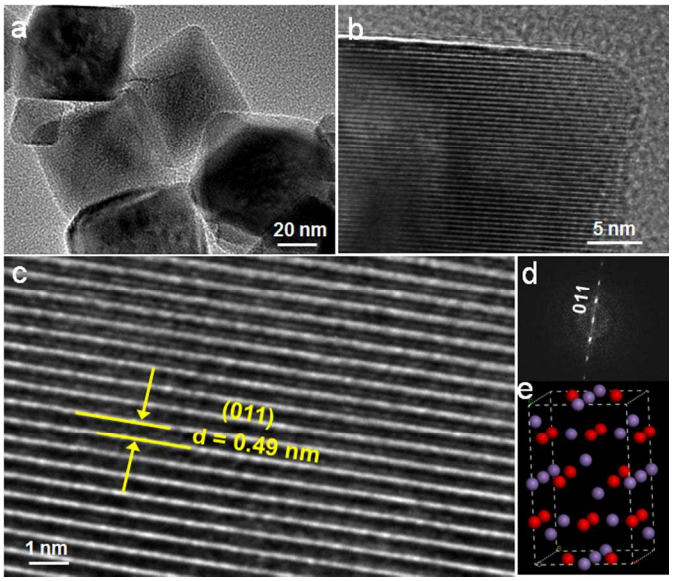

Fig. 2 a-b) Low-magnification TEM images of the as-prepared Mn_3O_4 nano-octahedrons. c-d) HRTEM image and the corresponding FFT of Mn_3O_4 nano-octahedrons. e) Tetragonal crystal structure of Mn_3O_4.

3.2 Growth process and the role of ethylenediamine

To understand the growth process of the Mn_3O_4 nano-octahedrons, the morphological evolution of the Mn_3O_4 nanoparticles was investigated. In the beginning, when $Mn(NO_3)_2$ was just mixed with ethylenediamine (EDA), sphere-like particles with size larger than 100 nm were formed (**Figure 3a**). After hydrothermal treatment for 15 min, the particles developed a truncated bipyramid shape with rough surface (Figure 3b). When the reaction proceeded for 30 min, the product remained a similar shape as those formed at 15 min, but the surface of the particles became smoother (Figure 3c). Afterwards, the particles continued to grow along the direction perpendicular to the square base plane of the truncated bipyramid (Figure 3d), until well-defined nano-octahedral shape was formed at 4 hrs (Figure 3e). The nano-octahedron shape was well retained upon further increase of the reaction time to 12 h (Figure S3). The corresponding growth process of the nano-octahedrons was schematically shown in Figure 3f. The amount of EDA also affects the shape of the product significantly (**Figure 4**). For the reaction without EDA, nanowires were observed (Figure 4a). With an EDA/$Mn(NO_3)_2$ ratio of 0.5, the product consisted of both nanowires and nano-octahedrons (Figure 4b). Nano-octahedrons without nanowires were obtained at EDA/$Mn(NO_3)_2$ ratios larger than 1.0 (Figure 4c, d).

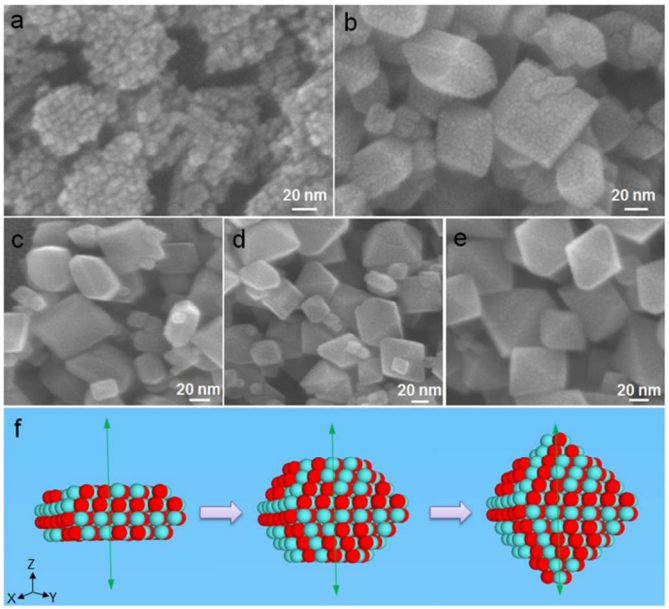

Fig. 3 a-e) FESEM images of the products collected at different reaction times: a) 0 min, b) 15 min, c) 30 min, d) 1.5 h and e) 4 h. Other reaction conditions: ratio of EDA/$Mn(NO_3)_2$ = 1.0; 180 °C. f) Schematic illustration of the growth process.

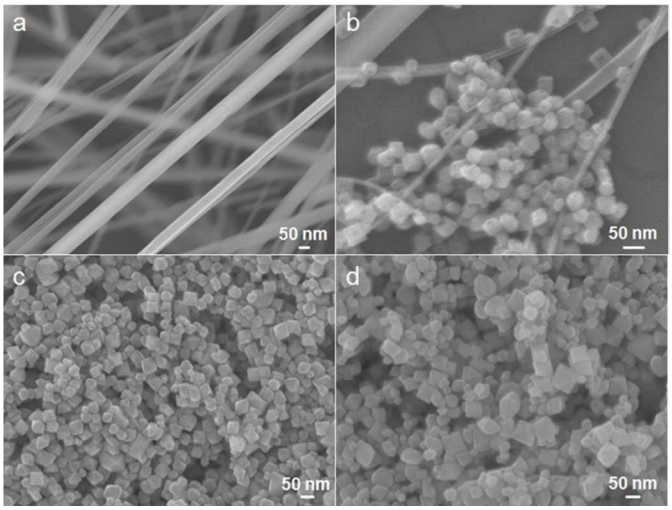

Fig. 4 FESEM images of the products obtained with different ratios of EDA/$Mn(NO_3)_2$: a) 0, b) 0.5, c) 1.0 and d) 2.5. Other reaction conditions: 180 °C, reaction time = 4 h.

The products collected at different reaction times and different EDA/$Mn(NO_3)_2$ ratios were examined with XRD. Particles obtained at 0 min are mainly monoclinic γ-MnOOH structure;[36] while for reaction times ranging from 15 min to 4 h, the Mn_3O_4 particles exhibit spinel structure (**Figure 5a**). If EDA was not added to the reaction, the resultant nanowires show a monoclinic γ-MnOOH structure (Figure 5b). At a EDA/$Mn(NO_3)_2$ ratio of 0.5, the product consisted of both monoclinic γ-MnOOH and spinel Mn_3O_4. Pure spinel Mn_3O_4 was obtained from the sample with a EDA/$Mn(NO_3)_2$ ratio of 1.0. These results reveal that EDA plays a critical role in formation of the Mn_3O_4 nano-octahedrons, not only to tailor the shape but also to affect the crystal structure of the products.

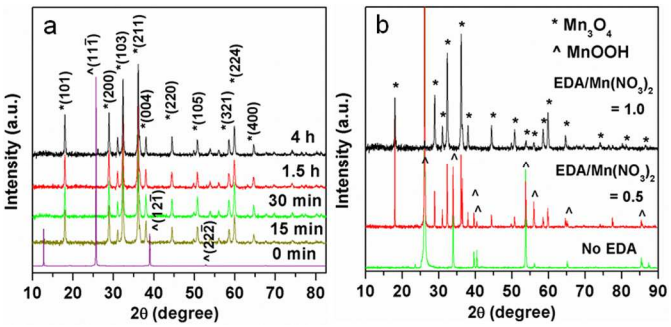

Fig. 5 XRD patterns of the as-synthesized materials at a) different reaction times and b) different ratios of $EDA/Mn(NO_3)_2$.

Based on the above experimental results, the growth process of the Mn_3O_4 nano-octahedrons was proposed to follow a "dissolution-recrystallization" and "capping-molecule assisted growth" mechanism.[37-39] At the beginning of the reaction, monoclinic γ-MnOOH nanocrystallites started to nucleate. To minimize the overall energy of the system, small nanoparticles were assembled to form sphere-like larger particles. As the reaction continued, the sphere-like γ-MnOOH particles disappeared while spinel Mn_3O_4 truncated octahedrons started to form, demonstrating the "dissolution-recrystallization" process. When the reaction proceeded further, the truncated Mn_3O_4 octahedrons grew along the direction perpendicular to the square base plane mediated by EDA molecules, eventually leading to the formation of nano-octahedrons via a "capping-molecule assisted growth" process.[40-42] Such a growth cannot be observed for the reaction without the use of EDA, indicating that EDA plays an important role in dictating the shape evolution during the synthesis. It was found that after adding EDA to the reaction, the initial pH of the solution was increased from 7.0 to 9.5. Due to the base nature of EDA, MnOOH was formed. In addition, EDA with amine groups can coordinate with Mn ions to form complexes, which can tailor the growth rate of Mn_3O_4 by binding to crystal facets, a phenomenon typically observed for capping agent-guided growth of nanocrystals.[43,44] During the hydrothermal treatment, MnOOH and Mn^{2+} were reconstructed to give Mn_3O_4 and grew with the mediation of EDA, resulting in the formation of 50-nm Mn_3O_4 nano-octahedrons. By optimizing the reaction conditions and exploring other structure-mediating agents, it is possible to further reduce the size of Mn_3O_4 nano-octahedrons.

3.3 Oxygen evolution reaction (OER) test

We further investigated the electrochemical activity of the 50-nm Mn_3O_4 nano-octahedrons as an electrocatalyst towards OER; and the performance was compared with Nafion+XC72 carbon black (binder and conductive additive) and larger Mn_3O_4 octahedrons with a size of 160 nm. FESEM image of the 160-nm Mn_3O_4 octahedrons prepared following a previous work[26] was given in Figure S4. To differentiate the different sizes, the 50-nm and 160-nm Mn_3O_4 octahedrons are shorten as "N-Mn_3O_4" and "Mn_3O_4", respectively. **Figure 6a** shows the OER polarization curves of N-Mn_3O_4, Mn_3O_4 and Nafion+XC72 in 0.1 M KOH electrolyte at a rotation speed of 1600 rpm and a scan rate of 5 mV s^{-1}. N-Mn_3O_4 displays a much higher capacitive current, indicating its larger electrochemically active surface area relatively to Mn_3O_4 and Nafion+XC72.[45,46] For the analysis of OER activities, the capacitive current was subtracted from the overall current at all potentials. The resulting current densities at overpotentials ($E_{vs.\ RHE}$ - 1.23V) from 0.37 to 0.57 V were plotted in Figure 6b. It clearly shows that at all overpotentials, the OER current densities of N-Mn_3O_4 are much higher than that of both Nafion+XC72 carbon black and 160-nm Mn_3O_4. Specifically, at an overpotential of 0.57 V, N-Mn_3O_4 provides an OER current density of 8.36 mA cm^{-2}, more than twice of that of 160-nm Mn_3O_4 (3.39 mA cm^{-2}); and over ten times of that of Nafion+XC72 carbon black (0.82 mA cm^{-2}). Tafel plots derived from the measurements in Figure 6a were given in Figure 6c. For N-Mn_3O_4, the Tafel slope is 71.5 mV dec^{-1}, which is much lower than that of 160-nm Mn_3O_4 (102.3 mV dec^{-1}), demonstrating much improved electrocatalytic activity of the 50-nm Mn_3O_4 octahedrons than larger ones. The OER performance of N-Mn_3O_4 is also compared with that of some recently reported Ni-, Pt-, Ir- and Ru-based catalysts.[47-49] At a current density of 5 mA cm^{-2}, the corresponding over-potenital for the 50-nm Mn_3O_4 nano-octahedrons is 0.46 V, lower than that of Pt/carbon catalyst (0.52 V)[49] and anodized Ni/carbon/Ni foam catalyst (0.48 V)[47]. While this over-potential is higher than that of Ru/carbon (0.38 V) and Ir/carbon catalysts (0.39 V),[49] the N-Mn_3O_4 offers its unique advantage of low cost. Stability of the electrodes was tested by linear potential sweep for 100 cycles and current density at an overpotential of 0.52V of each cycle was summarized in Figure 6d. Compared to 160-nm Mn_3O_4, the 50-nm Mn_3O_4 octahedrons provide much higher current densities at all cycles. After 100 cycles, the current retention for the 50-nm Mn_3O_4 is 96.7%, higher than 89.2% for 160-nm Mn_3O_4, indicating the good stability.

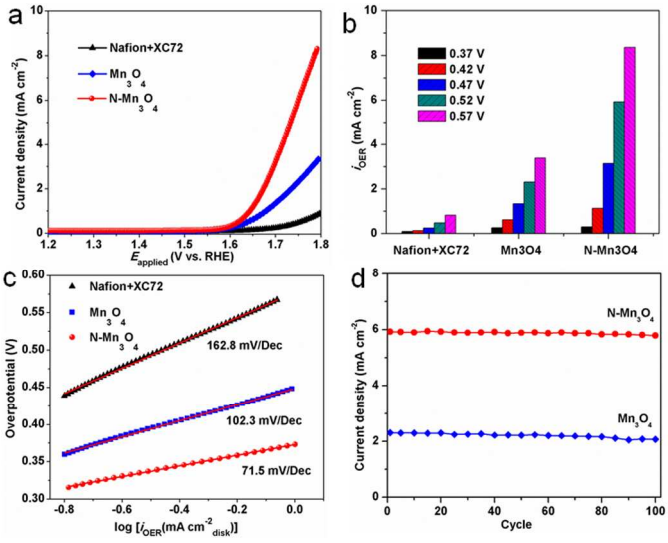

Fig. 6 a) OER linear potential sweep curves for Nafion + XC 72 carbon black, 160-nm Mn_3O_4 octahedrons (shorten as Mn_3O_4), and 50-nm Mn_3O_4 nano-octahedrons (shorten as N-Mn_3O_4). Electrolyte: 0.1 M KOH; sweep rate: 5 mV s^{-1}; rotation speed: 1600 rpm. b) The corresponding current densities at various overpotentials. c) Tafel plots derived from a) for the three materials. d) Stability of the electrodes was tested by linear potential sweep for 100 cycles and current density at an overpotential of 0.52 V of each cycle was summarized.

4. Conclusions

Mn_3O_4 nano-octahedrons with sizes down to 50 nm were synthesized using a hydrothermal method with $Mn(NO_3)_2$ as the manganese source and EDA as the structure-mediating agent. It

is found that ethylenediamine plays an important role in the formation of Mn_3O_4 nano-octahedrons in regulating both the morphology and the crystal structure of the products. The growth process of the Mn_3O_4 nano-octahedrons is proposed to follow a "dissolution-recrystallization" and "capping-molecule assisted growth" mechanism. As an OER electrocatalyst, the 50-nm Mn_3O_4 nano-octahedrons demonstrate much higher current densities and better stability than 160-nm Mn_3O_4 octahedrons. The OER performance of the nano-octahedrons is comparable to that of Pt/carbon and anodized Ni/carbon/Ni foam catalysts. By reducing the particle size and/or combining Mn_3O_4 with other OER-active catalysts such as Co nanoparticles to form composites, this OER performance could be further improved. In addition to electrocatalysis, the Mn_3O_4 nano-octahedrons could be potentially used for other applications such as photocatalytic reactions and sensing.

Acknowledgements

We thank the financial support by Ministry of Education, Singapore (Grant# R279-000-391-112) and National Research Foundation CRP program (Grant# R279-000-337-281).

Notes and references

Department of Chemical & Biomolecular Engineering, National University of Singapore (Singapore).
E-mail: chelxm@nus.edu.sg

Electronic Supplementary Information (ESI) available: [High magnification FESEM image and XPS survey spectrum of Mn_3O_4 nano-octahedrons; FESEM images of 50-nm Mn_3O_4 nano-octahedrons obtained after 12 h reaction and 160-nm Mn_3O_4 octahedrons]. See DOI: 10.1039/b000000x/

1. F. Cheng, J. Shen, B. Peng, Y. Pan, Z. Tao and J. Chen, *Nat. Chem.*, 2011, **3**, 79-84.
2. Y. Zheng, Y. Jiao, Y. H. Zhu, L. H. Li, Y. Han, Y. Chen, A. J. Du, M. Jaroniec and S. Z. Qiao, *Nat. Commun.*, 2014, **5**, 3783.
3. J. J. Duan, S. Chen, S. Dai and S. Z. Qiao, *Adv. Funct. Mater.*, 2014, **24,** 2072-2078.
4. Q. L. Dai and J. K. Tang, *Nanoscale*, 2013, **5**, 7512-7519.
5. A. Gasparotto, D. Barreca, C. Maccato and E. Tondello, *Nanoscale*, 2012, **4**, 2813-2825.
6. T. D. Nguyen, *Nanoscale*, 2013, **5**, 9455-9482.
7. Z. C. Zhang, Y. Yang, F. Nosheen, P. P. Wang, J. C. Zhang, J. Zhuang and X. Wang, *Small*, 2013, **9**, 3063-3069.
8. B. Lim, M. Jiang, P. H. C. Camargo, E. C. Cho, J. Tao, X. Lu, Y. Zhu and Y. Xia, *Science*, 2009, **324**, 1302-1305.
9. X. Guo, W. Ye, H. Y. Sun, Q. Zhanga and J. Yang, *Nanoscale*, 2013, **5**, 12582-12588.
10. Y. W. Lee, D. Kim, J. W. Hong, S. W. Kang, S. B. Lee and S. W. Han, *Small*, 2013, **9**, 660-665.
11. Y. Li, H. Tan, X. Y. Yang, B. Goris, J. Verbeeck, S. Bals, P. Colson, R. Cloots, G. Van Tendeloo and B. L. Su, *Small*, 2011, **7**, 475-483.
12. L. Y. Zhang, C. X. Guo, Z. Cui, J. Guo, Z. Dong and C. M. Li, *Chem. Eur. J.*, 2012, **18**, 15693-15698.
13. C. X. Guo, L. Y. Zhang, J. Miao, J. Zhang and C. M. Li, *Adv. Energy Mater.*, 2013, **3**, 167-171.
14. Y. Xu, H. Wang, Y. Yu, L. Tian, W. Zhao and B. Zhang, *J. Phys. Chem. C*, 2011, **115**, 15288-15296.
15. Z. A. Qiao, Z. Wu and S. Dai, *ChemSusChem*, 2013, **6**, 1821-1833.
16. J. W. Lee, A. S. Hall, J.-D. Kim and T. E. Mallouk, *Chem. Mater.*, 2012, **24**, 1158-1164.
17. M. H. Oh, T. Yu, S.-H. Yu, B. Lim, K.-T. Ko, M.-G. Willinger, D.-H. Seo, B. H. Kim, M. G. Cho, J.-H. Park, K. Kang, Y.-E. Sung, N. Pinna and T. Hyeon, *Science*, 2013, **340**, 964-968.
18. N. Zhao, W. Nie, X. Liu, S. Tian, Y. Zhang and X. Ji, *Small*, 2008, **4**, 77-81.
19. D. M. Robinson, Y. B. Go, M. Mui, G. Gardner, Z. Zhang, D. Mastrogiovanni, E. Garfunkel, J. Li, M. Greenblatt and G. C. Dismukes, *J. Am. Chem. Soc.*, 2013, **135**, 3494-3501.
20. J. W. Xiao, L. Wan, X. Wang, Q. Kuang, S. Dong, F. Xiao and S. Wang, *J. Mater. Chem. A*, 2014, **2**, 3794-3800.
21. J. Duan, Y. Zheng, S. Chen, Y. Tang, M. Jaroniec and S. Qiao, *Chem. Commun.*, 2013, **49**, 7705-7707.
22. T. Rhadfi, J. Y. Piquemal, L. Sicard, F. Herbst, E. Briot, M. Benedetti and A. Atlamsani, *Appl. Catal., A*, 2010, **386**, 132-139.
23. K. Subramani, D. Jeyakumar and M. Sathish, *Phys. Chem. Chem. Phys.*, 2014, **16**, 4952-4961.
24. T. Yu, J. Moon, J. Park, Y. I. Park, H. B. Na, B. H. Kim, I. C. Song, W. K. Moon and T. Hyeon, *Chem. Mater.*, 2009, **21**, 2272-2279.
25. H. Wang, L.-F. Cui, Y. Yang, H. Sanchez Casalongue, J. T. Robinson, Y. Liang, Y. Cui and H. Dai, *J. Am. Chem. Soc.*, 2010, **132**, 13978-13980.
26. H. Jiang, T. Zhao, C. Yan, J. Ma and C. Li, *Nanoscale*, 2010, **2**, 2195-2198.
27. H. Huang, Q. Yu, X. Peng and Z. Ye, *Chem. Commun.*, 2011, **47**, 12831-12833.
28. W. S. Seo, H. H. Jo, K. Lee, B. Kim, S. J. Oh and J. T. Park, *Angew. Chem. Int. Ed.*, 2004, **43**, 1115-1117.
29. P. Q. Zhang, Y. G. Zhan, B. X. Cai, C. C. Hao, J. Wang, C. X. Liu, Z. J. Meng, Z. L. Yin and Q. Y. Chen, *Nano Res.*, 2010, **3**, 235-243.
30. L. Zhang, Q. Zhou, Z. Liu, X. Hou, Y. Li and Y. Lv, *Chem. Mater.*, 2009, **21**, 5066-5071.
31. L. Li, J. Liang, H. Kang, J. Z. Fang, M. Luo and X. Y. Jin, *Applied Surface Science*, 2012, **261**, 717-721.
32. J. Yin, F. Gao, Y. Wu, J. Wang and Q. Lu, *CrystEngComm*, 2010, **12**, 3401-3403.
33. C. X. Guo, S. Huang and X. Lu, *Green Chem.*, 2014, **16**, 2571-2579.
34. A. M. E. Raj, S. G. Victoria, V. B. Jothy, C. Ravidhas, J. Wollschlager, M. Suendorf, M. Neumann, M. Jayachandran and C. Sanjeeviraja, *Appl. Surf. Sci.*, 2010, **256**, 2920-2926.
35. K.-H. Chang, Y.-F. Lee, C.-C. Hu, C.-I. Chang, C.-L. Liu and Y.-L. Yang, *Chem. Commun.*, 2010, **46**, 7957-7959.
36. L. Zhang, X. Zhang, Z. Wang, J. Xu, D. Xu and L. Wang, *Chem. Commun.*, 2012, **48**, 7598-7600.
37. A. Sarkar and S. Mahapatra, *J. Chem. Sci.*, 2012, **124**, 1399-1404.
38. X. Hu, Y. Masuda, T. Ohji and K. Kato, *Cryst. Growth Des.*, 2009, **10**, 626-631.
39. F. Y. Cheng, J. Z. Zhao, W. Song, C. S. Li, H. Ma, J. Chen and P. W. Shen, *Inorg. Chem.*, 2006, **45**, 2038-2044.
40. T. Vetter, M. Iggland, D. R. Ochsenbein, F. S. Hänseler and M. Mazzotti, *Cryst. Growth Des.*, 2013, **13**, 4890-4905.
41. C. C. Yec and H. C. Zeng, *J. Mater. Chem. A*, 2014.
42. T. W. Hansen, A. T. DeLaRiva, S. R. Challa and A. K. Datye, *Acc. Chem. Res.*, 2013, **46**, 1720-1730.
43. T. T. Tran and X. Lu, *J. Phys. Chem. C*, 2011, **115**, 3638-3645.
44. X. Lu, M. S. Yavuz, H.-Y. Tuan, B. A. Korgel and Y. Xia, *J. Am. Chem. Soc.*, 2008, **130**, 8900-8901.
45. C. X. Guo, A. A. Chitre and X. Lu, *Phys. Chem. Chem. Phys.*, 2014, **16**, 4672-4678.
46. C. X. Guo and C. M. Li, *Energy Environ. Sci.*, 2011, **4**, 4504-4507.
47. J. Wang, H. X. Zhong, Y. l. Qin and X. b. Zhang, *Angew. Chem. Int. Ed.*, 2013, **52**, 5248-5253.
48. T. Reier, M. Oezaslan and P. Strasser, *ACS Catal.*, 2012, **2**, 1765-1772.
49. Y. Gorlin and T. F. Jaramillo, *J. Am. Chem. Soc.*, 2010, **132**, 13612-13614.